Parallel Helix Bundles and Ion Channels: Molecular Modeling via Simulated Annealing and Restrained Molecular Dynamics

Ian D. Kerr,* Ramasubbu Sankararamakrishnan,* Oliver S. Smart,‡ and Mark S. P. Sansom*
*Laboratory of Molecular Biophysics, The Rex Richards Building, University of Oxford, Oxford OX1 3QU United Kingdom, and ‡Department of Crystallography, Birkbeck College, University of London, London WC1E 7HX United Kingdom

ABSTRACT A parallel bundle of transmembrane (TM) α-helices surrounding a central pore is present in several classes of ion channel, including the nicotinic acetylcholine receptor (nAChR). We have modeled bundles of hydrophobic and of amphipathic helices using simulated annealing via restrained molecular dynamics. Bundles of Ala_{20} helices, with $N = 4$, 5, or 6 helices/bundle were generated. For all three N values the helices formed left-handed coiled coils, with pitches ranging from 160 Å ($N = 4$) to 240 Å ($N = 6$). Pore radius profiles revealed constrictions at residues 3, 6, 10, 13, and 17. A left-handed coiled coil and a similar pattern of pore constrictions were observed for $N = 5$ bundles of Leu_{20}. In contrast, $N = 5$ bundles of Ile_{20} formed right-handed coiled coils, reflecting loosened packing of helices containing β-branched side chains. Bundles formed by each of two classes of amphipathic helices were examined: (a) M2a, M2b, and M2c derived from sequences of M2 helices of nAChR; and (b) $(LSSLLSL)_3$, a synthetic channel-forming peptide. Both classes of amphipathic helix formed left-handed coiled coils. For $(LSSLLSL)_3$ the pitch of the coil increased as N increased from 4 to 6. The M2c $N = 5$ helix bundle is discussed in the context of possible models of the pore domain of nAChR.

INTRODUCTION

A parallel bundle of transmembrane (TM) helices surrounding a central pore is a structural motif present in several, although not all, classes of ion channel (Oiki et al., 1990; Montal, 1990). This motif is of particular importance with respect to the nicotinic acetylcholine receptor (nAChR) in which the central pore is formed by a bundle of five parallel helices (Unwin, 1989, 1993; Stroud et al., 1990; Sansom, 1992a, c). A similar motif may occur in other ion channel proteins. For example, the influenza M_2 channel is thought to consist of a bundle of four parallel helices (Sansom and Kerr, 1993). Parallel helix bundles are also formed by a number of channel-forming peptides (CFPs) that self-assemble within lipid bilayers to form transbilayer pores (Sansom, 1991). Such CFPs include, e.g., alamethicin (Sansom, 1993a, b) and *Staphylococcus aureus* δ-toxin (Mellor et al., 1988; Sansom et al., 1991). Furthermore, certain de novo designed synthetic peptides also act as CFPs via formation of bundles of highly amphipathic α-helices (Lear et al., 1988; Åkerfeldt et al., 1993; Kienker et al., 1994). Amphipathic CFPs have also been employed as elements of helix bundles assembled on a covalent peptide template (Montal et al., 1993; Grove et al., 1993) to create peptide channels of fixed subunit stoichiometry. To understand the molecular basis of ion channel function in all of these systems, it is important to model bundles of parallel TM helices, particularly in the absence of atomic resolution structures for such ion channel proteins.

One approach to exploring possible structures of bundles of parallel helices is to model specific ion channels. This has been undertaken for several systems, e.g.: (a) models of the nAChR pore (Furois-Corbin and Pullman, 1989; Eisenman and Alvarez, 1991; Montal et al., 1993); and (b) models of channels generated by CFPs (Raghunathan et al., 1990; Åkerfeldt et al., 1993). Such studies have yielded valuable insights into possible channel structure/function relationships. A complementary approach is to investigate possible general principles underlying specific channel structures. Such investigations extend studies on helix-helix interactions in: (a) simple helix dimers (Chou et al., 1984); (b) 4-helix bundle proteins (Chou and Carlacci, 1991); and (c) antiparallel helix bundles (Furois-Corbin and Pullman, 1986b) to an investigation of channel-like structures. The primary aims of our investigations are to determine: (a) how the general rules of helix packing may be applied to parallel helix bundles; and (b) whether the presence of potential H-bonding residues influences the geometry of parallel helix bundles. In this manner, we hope to isolate some of the factors underlying helix-helix interactions in the more complex channel models mentioned above.

Parallel helix bundles are related in structure to α-helical coiled coils. The latter have been widely investigated from a theoretical viewpoint (Cohen and Parry, 1990; Lupas et al., 1991; Phillips, 1992; Adamson et al., 1993; Seo and Cohen, 1993; Zhang and Hermans, 1993; Cohen and Parry, 1994). Furthermore, x-ray and related structural data are available for the coiled coils formed by the leucine-zipper GCN4 (O'Shea et al., 1991) and by related peptides (Lovejoy et al., 1993; Harbury et al., 1993; Rozzelle et al., 1994). Thus,

Received for publication 28 April 1994 and in final form 12 July 1994.

Address reprint requests to Dr. Mark S. P. Sansom, Laboratory of Molecular Biophysics, University of Oxford, The Rex Richards Building, South Parks Road, Oxford, OX1 3QU UK. Tel.: 44-865-2755371; Fax: 44-865-510454.

Abbreviations used: D, inter-helix separation; d, restraint distance; E, potential energy; ΔE, helix-helix interaction energy; ΔE_{ES}, helix-helix interaction energy, electrostatic component; ΔE_{VDW}, helix-helix interaction energy, van der Waals component; N, number of helices per bundle; Ω, helix crossing angle; P, coiled coil pitch; R, pore radius; *RMSD*, root mean square deviation; R_{SYM}, RMSD of N-fold rotational symmetry.

0006-3495/94/10/1501/15 $2.00

coiled coils provide some experimental and theoretical data against which to compare structure predictions for parallel TM helix bundles.

A number of different modeling methods have been employed to study packing of α-helices. For example, energy minimization techniques were applied to dimers of simple hydrophobic helices (Chou et al., 1984; Furois-Corbin and Pullman, 1986a). The latter authors extended this approach to bundles of helices as models of ion channel proteins (Furois-Corbin and Pullman, 1986b, 1987). More recently, simulated annealing via restrained molecular dynamics simulations (SA/MD) has been developed as a modeling tool and has been applied to GCN4 (Nilges and Brünger, 1991) and glycophorin TM helix (Treutlein et al., 1992) dimers. Simulations of GCN4 dimers enabled successful prediction of the subsequently determined x-ray structure (O'Shea et al., 1991; Nilges and Brünger, 1993). An advantage of SA/MD is that it enables exploration of a wider range of conformational space than is feasible using constant temperature molecular dynamics simulations.

In the current study, SA/MD is used to generate models of pores formed by parallel bundles of simple hydrophobic TM helices. These models are analyzed in terms of their geometric and energetic properties, with particular emphasis on helix packing and on the dimensions of the central pore. Simulations are extended to embrace simple amphipathic TM helices. A preliminary account of some of these results has appeared in abstract form (Kerr et al., 1994).

MATERIALS AND METHODS

Programs

Molecular dynamics (MD) simulations and model building were carried out using Xplor V3.1 (Brünger, 1992) with the CHARMM PARAM19 (Brooks et al., 1983) parameter set. Only those H atoms attached to polar groups were represented explicitly; apolar groups were represented using extended atoms. Display and examination of models was carried out using Quanta V3.2 (Molecular Simulations), and diagrams of structures were drawn using Molscript (Kraulis, 1991). Pore dimensions were calculated using HOLE (Smart et al., 1993). MD simulations were performed on Convex C2 and DEC 3000 400 computers. All other calculations were carried out on Silicon Graphics Indigo R3000 workstations.

Simulated annealing/molecular dynamics

The SA/MD method used is similar to that of Nilges and Brünger (1991) and has already been described in the context of modeling single TM helices (Kerr and Sansom, 1993). In Stage 1 of SA/MD a Cα, template is constructed corresponding to a bundle of N exactly parallel ($\Omega = 0°$), idealized (rise/residue = 1.5Å; 3.6 residues/turn) α-helices. Remaining backbone and side-chain atoms are superimposed on the Cα atoms of the corresponding residues. These atoms explode from the Cα atoms, the positions of which remain fixed throughout Stage 1. Annealing starts at 1000 K, during which weights for bond lengths and bond angles, and subsequently for planarity and chirality, are gradually increased. A repulsive van der Waals term is slowly introduced after an initial delay. Once the scale factors of these components of the empirical energy function reach their final values, the system is cooled from 1000 to 300 K, in steps of 10 K and 0.5 ps. During this cooling, the van der Waals radii were reduced to 80% of their standard values to enable atoms to pass by one another. Electrostatic terms are *not* included during Stage 1. Five structures are generated for each bundle.

Structures from Stage 1 are each subjected to four molecular dynamics runs (Stage 2), resulting in an ensemble of $5 \times 4 = 20$ final structures. Initial velocities are assigned corresponding to 500 K. Harmonic restraints are imposed on Cα atoms at the beginning of Stage 2 and are gradually relaxed as the temperature is reduced from 500 to 300 K. Distance restraints were also introduced at this point (see next section). On reaching 300 K, a 5-ps burst of constant temperature dynamics is performed, followed by 1000 steps of conjugate gradient energy minimization. During the latter burst of dynamics and energy minimization, no restraints are imposed on the positions of the Cα atoms.

During Stage 2 electrostatic interactions are introduced into the potential energy function. All main-chain atoms are assigned partial charges as defined by the PARAM19 parameter set. Partial charges on side-chain atoms of *polar* residues are gradually scaled up, from 0.05 to 0.4 times their full value, while the temperature is reduced from 500 to 300 K. A distance-dependent dielectric function was used, with a switching function to smoothly truncate distant electrostatic interactions. Note that in each case the final scale factor (0.4) for polar side-chain partial charges applied at the end of the 500–300 K cooling period is also used during the subsequent 5-ps burst of dynamics and energy minimization. This is intended to mimic electrostatic screening of side-chain charge-charge interactions within the transbilayer pore by water and counterions.

Distance restraints

Intra- and inter-helix distance restraints are imposed during Stage 2. Both classes of restraint are implemented using the Xplor NOE potential energy function:

$$E_{\mathrm{NOE}} = \min\left[E_{\mathrm{MAX}}, \frac{SK_{\mathrm{B}}T}{2\sigma^2}\right](d - d_{\mathrm{TARGET}})^2,$$

where $E_{\mathrm{MAX}} = 50$ kcal/mol, $S = 2.5$, and $\sigma = 1.0$ Å. In this expression, d is the distance between the two restrained pseudo-atoms and d_{TARGET} is the target distance for the restraint. Intra-helix restraints are used to maintain α-helical geometry and so act between the carbonyl O of residue $i + 4$ and the amide H of residue i. Target distances for these restraints are derived from α-helical H-bonding geometries observed in crystal structures of globular proteins (Baker and Hubbard, 1984).

Inter-helix distances restraints act between pairs of virtual atoms. These virtual atoms are defined as the geometric centers of two groups of Cα atoms, each group within one of a pair of helices. In describing the inter-helix restraints, models are named on the basis of the number of helices per bundle and the number of distance restraints per helix. For example, A_{20}N2R3 corresponds to an A_{20} dimer with three inter-helix distance restraints. For dimers, N2R1 and N2R3 models were explored. N2R1 models had only one distance restraint linking the constituent monomers, whereas N2R3 had three such restraints. The exact nature of the restraints is given in Table 1, in which, e.g., Cα:3–9 implies the geometric center of the Cα atoms of residues 3–9. In Table 1, distance restraints from helix i to helix j are given as H_i to H_j. Note that the pattern of restraints is cyclic. Thus, for a bundle of five helices, H_i to H_{i+1} implies restraints linking helix 1 to 2, 2 to 3, 3 to 4, 4 to 5, *and* 5 to 1. Target distances for *adjacent* helices (i.e., H_i to H_{i+1}) are $d_{\mathrm{TARGET}} = 9.4$ Å unless specified otherwise in Results. Target distances *across* a bundle (i.e., H_i to H_{i+2} or H_{i+3}) are obtained from these distances by simple geometry. Studies on a number of helix bundle systems (J. Breed and M. S. P. Sansom, unpublished observations) suggest that the final structures from SA/MD are not over-dependent on the value of d_{TARGET} employed.

Analysis of structures

Helix crossing angles (Ω) were determined as described by Chothia et al. (1981). Inter-helix separations between adjacent helices of a bundle (D) were determined by calculating the distance between a pair of virtual atoms

TABLE 1 Inter-helix restraints

Model	Restraints
N2R1	H_i(Cα:10–16) to H_{i+1}(Cα:10–16)
N2R3	H_i(Cα:3–9) to H_{i+1}(Cα:3–9) H_i(Cα:10–16) to H_{i+1}(Cα:10–16) H_i(Cα:17–20) to H_{i+1}(Cα:17–20)
N5R1	H_i(Cα:8–14) to H_{i+1}(Cα:8–14)
N5R3	H_i(Cα:3–9) to H_{i+1}(Cα:3–9) H_i(Cα:8–14) to H_{i+1}(Cα:8–14) H_i(Cα:15–21) to H_{i+1}(Cα:15–21)
N5R6 & N4R6	H_i(Cα:3–9) to H_{i+1}(Cα:3–9) H_i(Cα:8–14) to H_{i+1}(Cα:8–14) H_i(Cα:15–21) to H_{i+1}(Cα:15–21) H_i(Cα:3–9) to H_{i+2}(Cα:3–9) H_i(Cα:8–14) to H_{i+2}(Cα:8–14) H_i(Cα:15–21) to H_{i+2}(Cα:15–21)
N6R6	H_i(Cα:3–9) to H_{i+1}(Cα:3–9) H_i(Cα:8–14) to H_{i+1}(Cα:8–14) H_i(Cα:15–21) to H_{i+1}(Cα:15–21) H_i(Cα:3–9) to H_{i+3}(Cα:3–9) H_i(Cα:8–14) to H_{i+3}(Cα:8–14) H_i(Cα:15–21) to H_{i+3}(Cα:15–21)

defined, in each helix, by the geometric centre of the Cα atoms of the helix. Ensemble averages of Ω and D were determined across all adjacent helix pairs within an ensemble. The pitch of coiled coils was determined as described by Seo and Cohen (1993; Method 2). Helix-helix interaction energies were calculated as

$$\Delta E = E_{\text{BUNDLE}} - \left(\sum_i^N E_i\right),$$

where E_{BUNDLE} is the potential energy of the intact bundle, E_i is the potential energy of constituent helix i in isolation, and where summation is over the N helices of the bundle.

An important aspect of analysis of SA/MD-generated structures is determination of the variation in geometrical and energetic parameters *within* an ensemble. Such variation should not be viewed as a failure to converge, but rather as an indication of the shape of the potential energy surface in the vicinity of the average structure. Indeed, one might employ the transformation described by, e.g., Sippl (1990) to obtain empirical potentials from such parameter distributions, which describe the geometry of helix bundles. Thus, measurements of ensemble parameter distributions provide an indication of how tightly the helices of a bundle interact.

For display of structures and calculation of pore radii (see below), it was convenient to select a representative structure for each ensemble. Because ion channels are quasi-symmetrical about the pore axis (Unwin, 1989, 1993), it was decided to select the structure with the highest degree of rotational symmetry. Members of an ensemble were ranked in order of their N-fold rotational symmetry by evaluation of

$$R_{\text{SYM}} = \frac{1}{N}\sum_{i=1}^{N-1} RMSD_i.$$

$RMSD_i$ is the α-carbon RMSD (after superposition of structures) between a bundle structure and the same structure in which helix 1 is relabeled as helix $1+i$, helix 2 as helix $2+i$, i.e., with the helix labels permuted in a circular fashion. Summation is over the $N-1$ such circular permutations of the labeling of N helices. The radius of the pore through helix bundles was determined by HOLE (Smart et al., 1993) using the van der Waals atomic radii of Weiner et al. (1984). Pore radii are displayed as a function of the distance moved parallel to the axis of rotational symmetry of the Cα template (z), thus generating pore radius profiles.

RESULTS

Helix dimers

SA/MD was used to generate dimers of hydrophobic TM helices. The aims of this were: (a) to evaluate the potential of the methodology; (b) to investigate the use of distance restraints to guide helix packing; and (c) to analyze helix packing within dimers to provide a comparison with helix bundles. Simple hydrophobic helices were used so as to facilitate comparison of our results with: (a) earlier studies of packing of Ala_N and related helices (Chou et al., 1984; Furois-Corbin and Pullman, 1986a, b); and (b) recent studies of formation of H^+-permeable channels in lipid bilayers by poly-Ala and poly-Leu (Oliver and Deamer, 1994).

Three hydrophobic TM helix sequences were used: Ac-A_{20}-NH_2, Ac-L_{20}-NH_2, and Ac-I_{20}-NH_2. The I_{20} sequence was included as Li and Deber (1992, 1994) have shown that β-branched side chains are helix-promoting when present in a bilayer environment. The N- and C-termini are blocked with an acetyl group and an amide group, respectively, so as to mimic the effects of preceding and following peptide bonds within an intact protein. The initial inter-axial separation of the helices was 9.4 Å (based on analysis of helix-helix packing in globular proteins (Chothia et al., 1981; Chothia, 1984). Helices were initially oriented such that they were related by a twofold axis running parallel to and midway between the helix axes. Thus, the helices were exactly parallel, i.e., the initial crossing angle was Ω = 0°. These initial models consisted of Cα templates corresponding to ideal α-helices with a rise/residue of 1.5 Å and 3.6 residues/turn (Schulz and Schirmer, 1979).

When generating helix dimers via SA/MD inter-helix distance restraints were included, to prevent the two helices from drifting apart. This was carried out in a similar fashion to that described by Nilges and Brünger (1991), i.e., a NOE-like distance restraint was employed (see Materials and Methods for details). For each sequence, two patterns of restraints were investigated: (a) one restraint per helix pair (N2R1, see Table 1); and (b) three restraints per helix pair, acting between the N-termini, the centers, and the C-termini of the helices (N2R3, see Table 1). For each model an ensemble of 50 structures was generated, corresponding to 10 runs of stage I and 10 × 5 runs of stage II.

Fig. 1, *A* and *C* illustrate 10 structures, each selected from the A_{20}N2R1 and A_{20}N2R3 ensembles, shown as Cα traces. It is evident that there is variation within an ensemble and that this variation is somewhat greater for the N2R1 ensemble. However, the structures are all broadly similar. In particular, they all exhibit a positive helix crossing angle (Ω; Chothia, 1984), as illustrated for single members of the same two ensembles in Fig. 1, *B* and *D*. This confirms that SA/MD is able to generate structural features *not* included in the initial Cα template.

A summary of the results obtained for the six ensembles of hydrophobic helix dimers is given in Table 2. Comparing the results for the A_{20}N2R1 and A_{20}N2R3 models, it can be

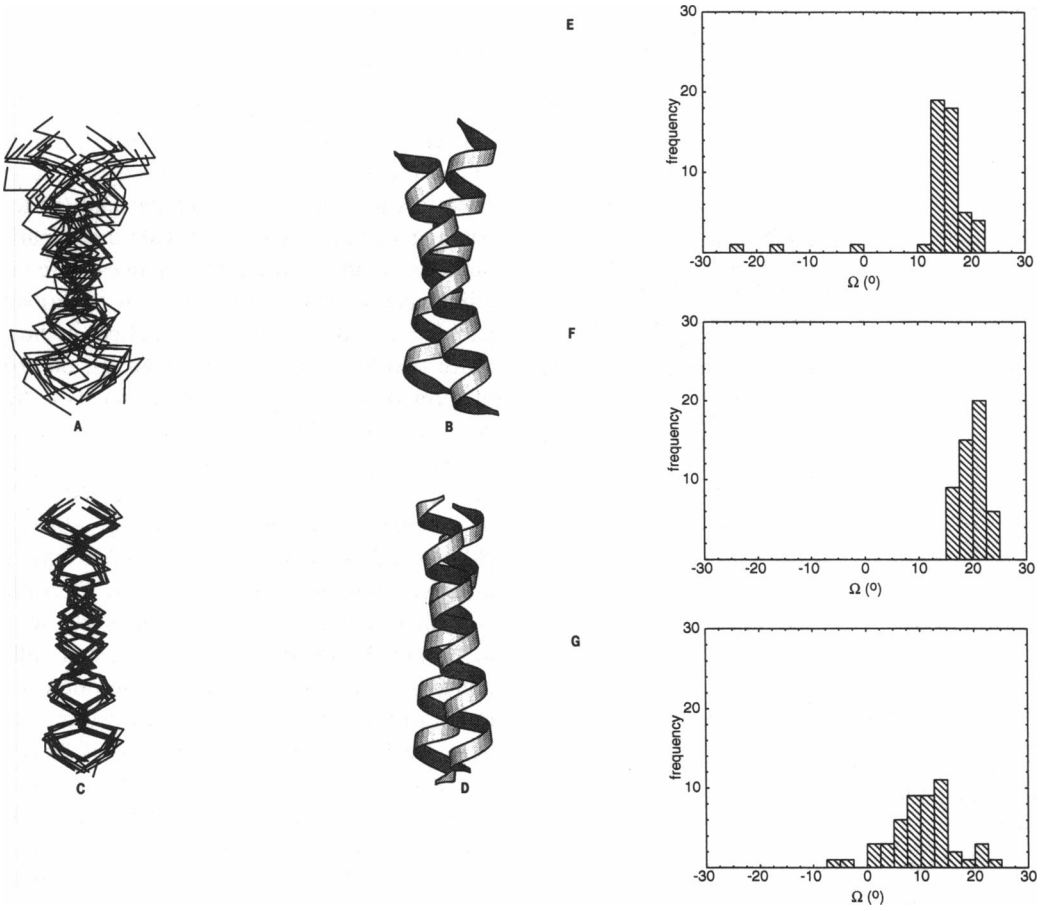

FIGURE 1 Helix dimers. *A* shows A_{20}N2R1 structures selected from an ensemble of 50 generated. The Cα backbones of the helices are shown superimposed. *B* shows a representative structure from the same ensemble, selected such that its crossing angle is equal to the mean for the ensemble ($\langle\Omega\rangle$ = +26°). *C* and *D* are the corresponding diagrams for the A_{20}N2R3 ensemble. *E*, *F*, and *G* show the distributions of helix crossing angles for A_{20}, L_{20}, and I_{20} N2R3 ensembles, respectively. In each case, an ensemble of 50 structures was generated.

TABLE 2 Helix dimers

Model	RMSD* (Å)	$\langle\Omega\rangle$ (°)	$\langle D\rangle$ (Å)	$\langle P\rangle$ (Å)	$\langle\Delta E_{VDW}\rangle$ (kcal/mol)	%χ_1 g^+	t	g^-
A_{20}N2R1	1.8	+27 (18)	8.2 (0.7)	163 (157)	−18 (6)			
A_{20}N2R3	1.3	+14 (8)	7.8 (0.4)	108 (237)	−23 (3)			
L_{20}N2R1	0.7	+26 (6)	9.4 (0.3)	142 (29)	−36 (4)	53	45	2
L_{20}N2R3	0.4	+20 (2)	9.2 (0.1)	174 (30)	−39 (1)	52	46	2
I_{20}N2R1	1.5	+26 (15)	10.3 (0.3)	40 (2350)	−21 (5)	71	6	23
I_{20}N2R3	0.8	+10 (6)	9.6 (0.2)	346 (1030)	−30 (3)	69	8	22

* The RMSD values refer to backbone atoms (i.e., N, Cα, C, and O) only.

seen that in both cases the helices pack with a positive mean crossing angle, at an inter-helix separation of ~8 Å. This is close to the anticipated crossing angle of Ω = +23° described by Chothia (1984) for class 3–4 ridges-in-grooves helix packing. However, comparison of the SDs of Ω and *D* suggest that there is much greater variability for the N2R1 ensemble than for the N2R3 ensemble. It appears, therefore, that using three restraints per helix results in a less disparate ensemble of models. This is confirmed by comparison of the main-chain RMSDs. Furthermore, because the aim of this study is to model helix dimers constrained to pack in an approximately parallel fashion by their presence within a lipid bilayer, the imposition of the additional distance restraints so as to favor such models is justified. Examination of the interaction energies reveals that the mean interaction energy (ΔE_{VDW}) is lower for the N2R3 ensemble than for the corresponding N2R1 ensemble. Similar results were obtained for the N2R3 and N2R1 ensembles for L_{20} and I_{20} ensembles.

It is also informative to consider the variation in crossing angles within a given ensemble. The distributions of Ω for the N2R3 ensembles of A_{20}, L_{20}, and I_{20} are given in Fig. 1,

E, *F*, and *G*, respectively. The distribution for A_{20} is still relatively broad, indicating that the use of three restraints does not force the final structure, with a mode of $\Omega \sim +15°$, i.e., reasonably close to the theoretical 3–4 crossing angle. The distribution for L_{20} is centered about $\Omega = +20°$, and is somewhat less disperse. The distribution for I_{20} peaks in the vicinity of $\Omega = +15°$, but is much broader than that for A_{20}. Thus, even at the level of helix dimers there is a difference in the preferred packing of I_{20} and the other two hydrophobic helices.

Differences in packing of the three different sequences are also reflected in their coiled coil pitches. Note that a positive crossing angle results in a left-handed coiled coil (i.e., $P > 0$). For both A_{20} and L_{20}, the N2R3 ensembles have mean pitches of ~170 Å, whereas for I_{20} this is increased to ~350 Å. Furthermore, the SD of the pitch is much greater in the latter case.

Also tabulated are the torsion angles (χ_1) for the side chains of the L_{20} and I_{20} dimers. For the L_{20} dimers, most side chains were in the preferred conformations (i.e., g^+ or t; McGregor et al., 1987). For both ensembles, the ratio of t:g^+ was ~1:1 (cf. 4:6 for high resolution x-ray structures of proteins; McGregor et al., 1987). The unfavorable g^- conformation was largely absent. For the I_{20} dimers, the χ_1 distribution shifted towards the g^- conformation. This is consistent with modeling studies of isoleucine in GCN4-like coiled coils, which suggest that isoleucine adopts less favored conformations at helix-helix interfaces (Harbury et al., 1993).

Overall, studies on hydrophobic TM helices suggest that both A_{20} and L_{20} form dimers exhibiting classical ridges-in-grooves helix packing. The larger side chains of L_{20} result in tighter helix-helix interactions, as evidenced by a more negative ΔE_{VDW} and by a narrower Ω distribution. In contrast, the β-branched side chains of I_{20} result in looser helix packing. Furthermore, the Ile side chains are perturbed from their preferred rotamers at the helix-helix interface. This suggests that β-branched side chains in TM helices might play a role in modulating the geometry of helix-helix interactions.

N = 5 A_{20} helix bundles

Ion channels are believed to be formed by approximately symmetrical bundles of parallel helices. To investigate the necessary inter-helix distance restraints for generating symmetrical bundles, ensembles of $N = 5$ A_{20} helix bundles were generated with 1, 3, and 6 such restraints per helix (i.e., N5R1, N5R3, and N5R1, see Table 1). The primary aim of these investigations was to determine which pattern of restraints was optimal for generating helix bundles with a central pore comparable with those thought to be present in ion channels.

Cα templates were constructed from exactly symmetrical bundles of five parallel ($\Omega^- = 0°$) helices. The interaxial separation of the helices was 9.4 Å. These templates were used in SA/MD to generate ensembles of 20 structures for each model, corresponding to 5 runs of Stage 1 and 5 × 4 runs of Stage 2.

N5R1 and N5R3 ensembles were generated, in both cases using $d_{TARGET} = 9.4$ Å. The geometric and energetic properties of these are summarized in Table 3, from which it can be seen that there is no significant difference in the results, other than slightly smaller SDs for the Ω and D distributions for the N5R3 ensemble. Consequently, subsequent discussion focus on the N5R3 ensemble. For both the N5R1 and N5R3 ensembles, it was also found that only 1 of the 20 structures generated corresponded to an approximately symmetrical bundle of helices surrounding a central pore. This can be seen in Fig. 2 *A*, where the 20 members of the N5R3 ensemble are represented. Using the R_{SYM} analysis described above, the structure labeled α was shown to be the most symmetrical bundle, with an open pore.

On this basis, it was decided to use further inter-helix restraints to generate a larger population of open bundles. One way of achieving this would have been to apply symmetry constraints, but we were concerned that this might impose too severe a restriction on helix packing. Instead, an additional three restraints per helix (at the N-terminus, center, and C-terminus) were imposed, yielding six restraints per helix in total. The additional distance restraints acted *across* the bundle (i.e., N5R6, see Table 1). Target distances for the latter set of restraints were calculated on the basis of ideal pentagonal geometry. In the N5R6 model, the i, $i + 1$ restraints used a target distance of $d_{TARGET} = 8.1$ Å (on the basis of results with A_{20} dimers and with the previously described A_{20} bundles), and the i, $i + 2$ restraints used $d_{TARGET} = 13.1$ Å. Again, an ensemble of 5 × 4 structures was generated.

TABLE 3 Hydrophobic TM helix bundles

Model	⟨Ω⟩ (°)	⟨*D*⟩ Å	⟨ΔE_{VDW}⟩ (kcal/mol)	%χ_1^*		
				g^+	t	g^-
A_{20}N5R1	+10 (14)	8.5 (0.6)	−105.7 (6.9)			
A_{20}N5R3	+14 (10)	8.2 (0.5)	−109.5 (8.3)			
A_{20}N5R6	+13 (2)	7.9 (0.2)	−120.5 (13.6)			
A_{20}N4R6	+10 (12)	8.1 (0.4)	−91.1 (10.1)			
A_{20}N6R6	+11 (6)	8.1 (0.3)	−127.0 (5.0)			
L_{20}N5R6	+13 (2)	9.7 (0.2)	−199.7 (5.5)	48	39	1
I_{20}N5R6	−1 (5)	10.3 (0.2)	−132.1 (6.5)	63	6	28

* Values of χ must fall within ±30° of the canonical values for a side chain to be defined as g^+, t, or g^-.

A schematic diagram of the N5R6 ensemble is given in Fig. 2 *B*. It can be seen that all 20 members of the ensemble form approximately symmetrical helix bundles. Using the R_{SYM} analysis to rank the members of the ensemble in order of symmetry, it was shown that both the least and the most symmetrical bundles were open, i.e., possessed an unoccluded central pore running through the center of the bundle.

It is also informative to compare the geometric and energetic properties of the N5R3 and N5R6 ensembles (Table 3 and Fig. 2, *C* and *D*). There is no significant difference in the mean values of Ω and *D* for the two ensembles. However, the range of crossing angles is considerably reduced for the N5R6 ensemble. The mean of $\Omega = +13°$ for the $N = 5$ bundles corresponds very closely to the mean value for the A_{20}N2R3 ensemble of dimers. Thus, the $N = 5$ bundle also exhibits left-handed coiling of the helices (see below). Interestingly, the van der Waals component of the helix interaction energy is somewhat lower for the N5R6 ensemble. This suggests that additional inter-helix restraints favor formation of a tighter packing arrangement during the SA/MD simulation, as also indicated by the narrower range of Ω values. Helix interaction energies are just over 5 times those for the A_{20} dimers, also supporting the proposal that packing in the bundle is similar to that in the dimer.

A_{20} $N = 4$, 5, and 6 bundles compared

Having established a protocol for generation of symmetrical, open bundles, it was employed to generate bundles with different stoichiometries. In particular, it was of interest to examine whether helix packing changed with number of helices and, also, how the pore dimensions changed. Accordingly, $N = 4$ and 6 bundles of A_{20} helices were generated in the same manner as for A_{20}N5R6 (i.e., A_{20}N4R6 and A_{20}N6R6, Table 1).

First, let us examine the $N = 5$ bundle in more detail. Fig. 3 is a schematic representation of the most symmetrical member of the ensemble (labeled α in Fig. 2 *B*). It can be seen that the positive crossing angles of the helices ($\langle\Omega\rangle = +12°$; Table 6) result in an overall bundle corresponding to a left-

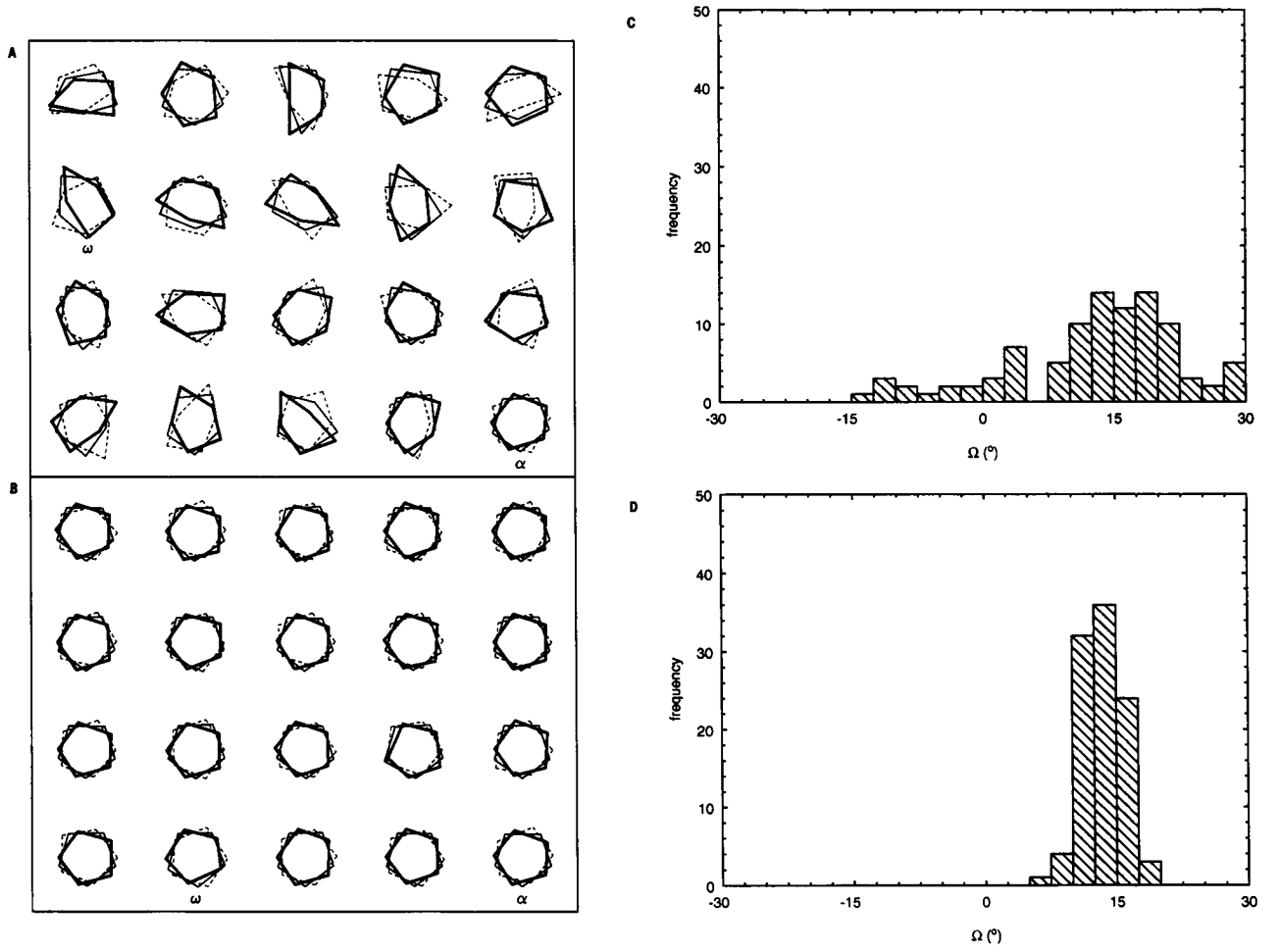

FIGURE 2 A_{20} helix bundles, $N = 5$. *A* and *B* illustrate ensembles of 20 structures of A_{20}N5R3 and A_{20}N5R6 helix bundles, respectively. Each bundle is represented by three pentagons, one corresponding to the N-termini of the helices (*bold lines*), one the center of the helices (*thin lines*), and one the C-termini (*dashed lines*). The columns correspond to the Stage 1 and the rows to the Stage 2 runs during generation of the ensemble of 5 × 4 structures. For each ensemble, the most and least symmetrical members are indicated by α and ω, respectively. *C* and *D* show the distribution of helix crossing angles for the A_{20}N5R3 and A_{20}N5R6 ensembles, respectively.

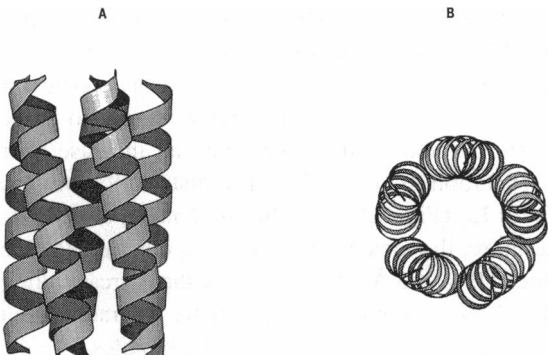

FIGURE 3 The most symmetrical $A_{20}N5R6$ helix bundle, displayed using helical ribbons. *A* shows the bundle viewed down a perpendicular to the pore (z) axis with the N-termini of the helices at the top of the diagram. *B* is a view along z from the N-termini towards the C-termini.

handed coiled coil, with mean pitch $\langle P \rangle = 234$ Å. The mean inter-helix separation, $\langle D \rangle = 7.8$ Å, indicates close packing of the constituent helices of the bundle. Examining the structure in more detail (Fig. 4 *B*) reveals that the Cβ atoms of the residues interdigitate to give ridges-in-grooves packing.

Fig. 4 displays the most symmetrical bundles from the $N = 4$ and 6 ensembles in addition to that for $N = 5$, and the corresponding geometric and energetic properties are summarized in Tables 3 and 6. It can be seen that for all three stoichiometries the *ensemble* mean of the helix crossing angles is ~+11°. However, consideration of the most symmetrical bundles (Table 6) reveals a small but significant trend in the bundle geometry as function of the number of helices. As N increases, Ω decreases (from +18° for $N = 4$ to +12° for $N = 5$ and 6), and the coiled coil pitch increases (from 161 to ~240 Å). A similar trend is observed in the LS helix bundles (see below) and in models of alamethicin channels (J. Breed and M. S. P. Sansom, unpublished observations). This suggest that although the same overall packing mode (3–4, corresponding to a left-handed coiled coil) is found in all three bundles, for higher N the requirement for a symmetrical bundle places additional constraints on helix packing. Despite this difference, the interaction energy per helix-helix interface, $\Delta E_{VDW}/N$, is independent of N. For the dimer, and for the $N = 4$, 5, and 6 ensembles $\Delta E_{VDW}/N = -22$, -23, -24, and -21 kcal/mol, respectively.

In the context of modeling possible structures of ion channels, it is important to estimate the dimensions of the central pores. This has been achieved by using HOLE (Smart et al., 1993), which determines the pore radius (R) as a function of the distance traveled parallel to the pore, i.e., z, axis. Note that this is achieved by allowing the center of the pore, for each z value, to move in the xy plane so as to maximize the size of a sphere within the van der Waals surface of the pore. This produces the radius profile and defines an irregular trajectory for the center of the pore. The results presented (Table 6 and Fig. 5) are for the most symmetrical member (as defined by the R_{SYM}) of each ensemble. However, the same analysis applied to the least symmetrical members of the same ensembles does not generate significantly different results.

The mean and minimum pore radii ($\langle R \rangle$ and R_{MIN}) reveal that the pore radius increases approximately linearly with the number of helices in the bundle, as one would expect. Thus, the $N = 4$ pore has a radius of ~1 Å and would not allow passage of, e.g., monovalent cations without significant distortion of the bundle. The $N = 6$ pore is wide enough to permit passage of fully hydrated ions. These differences are reflected in the variation in the mean deviation of the center of the pore from the z axis (~0.7, 0.2, and 0.3 Å for the $N = 4$, 5, and 6 bundles, respectively). The larger value

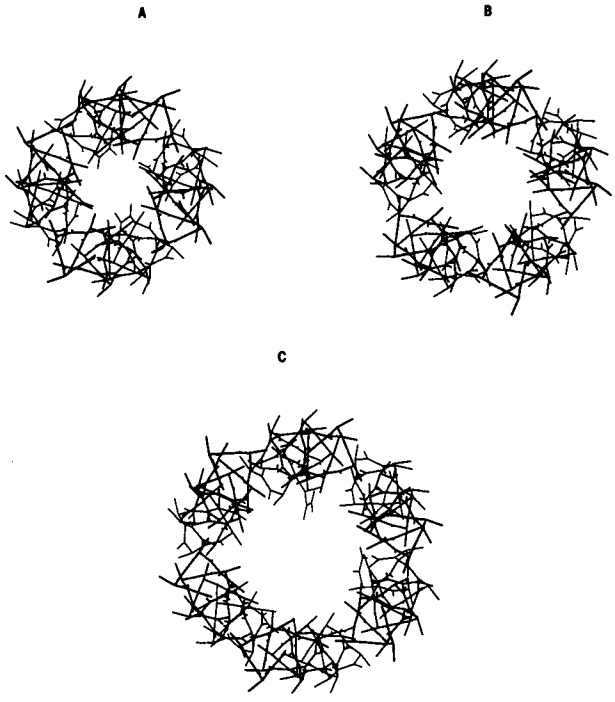

FIGURE 4 The most symmetrical $A_{20}N4R6$ (*A*), $A_{20}N5R6$ (*B*), and $A_{20}N6R6$ (*C*) bundles, viewed down z from the N-termini towards the C-termini of the helices.

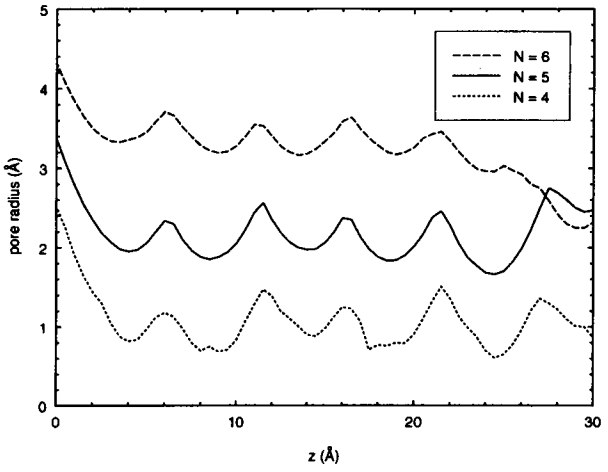

FIGURE 5 Pore radius profiles calculated using HOLE for the most symmetrical $A_{20}N4R6$, $A_{20}N5R6$, and $A_{20}N6R6$ helix bundles. The N-termini of the helices are at z ~0 Å and the C-termini at z ~30 Å.

of the mean deviation for the $N = 4$ bundle reflects the more labyrinthine trajectory of the center of the pore.

Of particular interest in the context of the pore-lining residues of ion channel proteins (Sansom, 1992; Bertrand et al., 1993) is the variation in the pore radius as a function of z (Fig. 5). For each of the three models, this reveals a pore running from $z \sim 0$ Å (the N-terminal mouth) to $z \sim 30$ Å (the C-terminal mouth), with a periodic variation in the pore radius. The closest contact atoms at the minima in the pore radius profile are, for all three models, the Cβ atoms of residues 3, 6, 10, 13, and 17. This 3- or 4-residue periodicity clearly reflects that of the constituent helices and indicates the positions at which one might expect to find pore-lining side chains in channel proteins. There is an additional constriction at the C-terminal mouth of the $N = 6$ pore, for which the closest contact is Cβ:20. As can be seen from Fig. 4 *C*, this is a result of the slight distortion of the C-terminus of one of the helices of the bundle.

L_{20} and I_{20} $N = 5$ bundles

$N = 5$ bundles of L_{20} and of I_{20} helices were generated (20 structures in each ensemble) using six distance restraints per helix (Tables 3 and 6). The $i,i+1$ restraints used d_{TARGET} values of 9.4 and 9.9 Å, respectively, based on the results with the corresponding helix dimers. The geometrical properties of the L_{20}N5R6 ensemble were similar to those for A_{20}N5R6, the major difference being an increase in interhelix separation to $D = 9.7$ Å. The distribution of crossing angles for L_{20} (Fig. 6 *A*) was almost identical to that for A_{20}. Furthermore, the most symmetrical L_{20} bundle had a coiled coil pitch ($P = 283$ Å) close to that of the corresponding A_{20} bundle ($P = 234$ Å). The helix-helix interaction energy (ΔE_{VDW}) was larger for L_{20} than for A_{20} bundles (~ -40 and -20 kcal/mol/helix, respectively). Comparison of L_{20} bundles with L_{20} dimers revealed a lower helix crossing angle and higher coiled coil pitch in the former. The distribution of side-chain torsion angles in the bundles was much the same as in the dimers, with the g^+ and t conformations favored.

I_{20} bundles differ markedly from A_{20} and L_{20} bundles. Their mean helix crossing angle is close to 0°, corresponding to parallel helices. The crossing angle distribution (Fig. 6 *B*) is much broader than for A_{20} and L_{20}, with Ω ranging from $\sim -12°$ to $+12°$. Indeed, the most symmetrical I_{20}

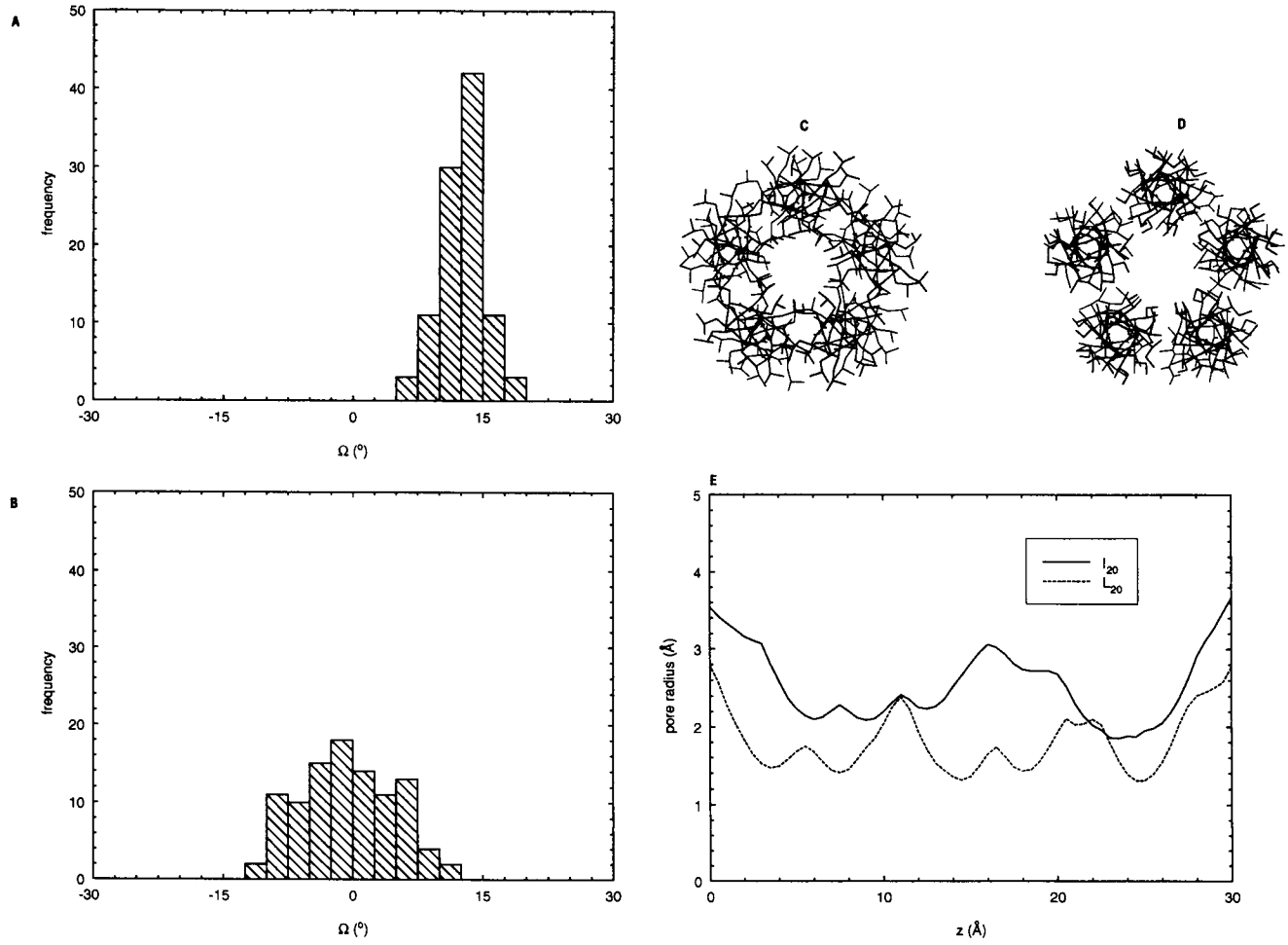

FIGURE 6 L_{20}N5R6 and I_{20}N5R6 helix bundles. *A* and *B* show the distributions of helix crossing angles for ensembles of 20 L_{20} and I_{20} bundles, respectively. *C* and *D* show the most symmetrical bundles from the L_{20} and I_{20} ensembles, respectively. *E* shows the pore radius profiles for the same two bundles. The N-termini of the helices are at $z \sim 0$ Å and the C-termini at $z \sim 30$ Å.

bundle (Table 6) has a mean crossing angle of −5°, corresponding to a right-handed coiled coil. It seems that the β-branched isoleucine side chains hinder efficient packing of the helices within the bundle. This is reflected in the increased mean helix-helix separation (10.3 Å) and decreased ΔE_{VDW} (~−26 kcal/mol/helix) relative to L_{20}. Difficulties of packing of I_{20} helices together are also revealed by adoption of the unfavorable g^- conformation by side chains at the helix-helix interfaces, as was also found for the I_{20} dimers.

The most symmetrical L_{20} and I_{20} $N = 5$ bundles are shown in Fig. 6, *C* and *D*. Failure of the β-branched side chains to fully interdigitate in the I_{20} bundle is evident. The corresponding HOLE trajectories are shown in Fig. 6 *E*. The L_{20} profile resembles that for the A_{20} bundle, with minima in the pore radius corresponding to the side chains of residues 3, 6, 10, 13, and 17. Interestingly, despite the greater helix-helix separation of the L_{20} bundle, the mean and minimum pore radii are less than for the A_{20} bundle. The minimum radius (R_{MIN} = 1.3 Å) of the L_{20} pore corresponds to, e.g., the crystal radius of a K^+ ion. The I_{20} pore is wider (R_{MIN} = 1.8 Å), and the HOLE profile does not exhibit as regular a pattern of minima as for L_{20}.

Overall, comparison of the $N = 5$ bundles of A_{20}, L_{20}, and I_{20} suggests that: (a) helix-helix packing in symmetrical, open bundles is equally tight for A_{20} and L_{20} helices, despite the larger side chains and, hence, stronger van der Waals interactions, in the latter; and (b) helix-helix packing is much looser in I_{20} bundles. The latter reflects the results with I_{20} dimers, in that β-branched side chains do not readily participate in ridges-in-grooves interdigitation.

Amphipathic helices

Several classes of ion channel are formed by bundles of *amphipathic* TM helices. Two types of sequence have been used to model bundles of amphipathic helices (Table 4). M2a, M2b, and M2c are derived from the sequence of the pore-lining M2 helix of the nicotinic acetylcholine receptor (nAChR; Stroud et al., 1990; Lester, 1992; Unwin, 1993). Site-directed mutagenesis (Leonard et al., 1988; Charnet et al., 1990; Villarroel et al., 1991), chemical labeling (Hucho et al., 1986; Giraudat et al., 1987; Changeux et al., 1992; Bertrand et al., 1993), and molecular modeling (Sansom, 1992) studies suggest that serine and/or threonine side chains at positions 4, 8, and 12 of nAChR M2 helices interact with ions as they pass through the channel. M2a and M2b are amphipathic analogs of A_{20} and L_{20} with serine residues at positions 4, 8, and 12. M2c is a consensus sequence derived by comparison of M2 helices from different nAChRs. However, unlike nAChR M2 sequences, M2c does not contain ionizable side chains near the termini of the helix. These were excluded to focus on properties of polar groups within the transbilayer region of M2.

It is important to consider whether M2a, M2b, and M2c would be expected to form α-helices within a bilayer. Recent work by Li and Deber (1994)) suggests that the amino acids Leu, Ile, Val, Phe, and Ala all have a high propensity for helix formation in the presence of SDS micelles or DMPG vesicles. Thus, given the amino-acid composition of the three M2-derived sequences (Table 4), it is highly likely that they would form helices in a bilayer environment. Of course, this could be evaluated experimentally by peptide synthesis combined with CD or FTIR spectroscopy.

The second type of amphipathic sequence (LS; Table 4) is that of the 21-residue, channel-forming peptide designed de novo by DeGrado and colleagues (Lear et al., 1988; DeGrado et al., 1989; Åkerfeldt et al., 1993). This has been shown to adopt an α-helical conformation in methanol and to form cation-selective channels in planar lipid bilayers. The alternation of leucine and serine residues within the sequence results in an ideal amphipathic helix. Previous modeling studies (Åkerfeldt et al., 1993) using an energy-minimization based technique, have examined N = 3, 4, 5, and 6 bundles of LS helices. The results of these studies may be compared with the results of SA/MD modeling described below.

M2a, M2b, and M2c: $N = 5$ bundles

The nAChR pore is formed by five M2 helices, one from each subunit. Therefore, $N = 5$ bundles of M2a, M2b, and M2c helices were modeled. Ensembles of 20 structures were generated for each sequence, using six distance restraints per helix. The Cα templates were constructed such that the center of the hydrophilic face of each helix, defined by the Cα atoms of S8, was directed towards the center of the bundle. Thus, the serine side chains formed the lining of the resultant pores, as can be seen in Fig. 7, *A–C*. The geometric and energetic properties of the ensembles are summarized in Table 5. The properties of the pores formed by the most symmetrical members of the ensembles are given in Table 6.

All three M2 helices formed bundles corresponding to a left-handed coiled coil. However, the mean crossing angles for the three M2 ensembles are all lower than those of either the A_{20} or L_{20} ensembles. For example, $\langle\Omega\rangle = +5.6°$ for M2b, compared with +13° for L_{20}, the corresponding hydrophobic TM helix. This difference between the amphipathic and hydrophobic helix bundles is most marked for M2a (*vs.* A_{20}N5R6) and least marked for M2c (*vs.* L_{20}N5R6).

TABLE 4 Amphipathic helix sequences

Helix	Sequence	Comments
M2a	Ac-A-A-A-*S*-A-A-A-*S*-A-A-A-*S*-A-A-A-A-A-A-A-A-NH_2	Simplified M2
M2b	Ac-L-L-L-*S*-L-L-L-*S*-L-L-L-*S*-L-L-L-L-L-L-L-L-NH_2	Simplified M2
M2c	Ac-L-L-I-*S*-L-A-I-*S*-V-L-L-*S*-L-*T*-V-F-L-L-L-I-NH_2	Simplified M2
LS	L-*S*-*S*-L-L-*S*-L-L-*S*-*S*-L-L-*S*-L-L-*S*-*S*-L-L-*S*-L-NH_2	Synthetic CFP

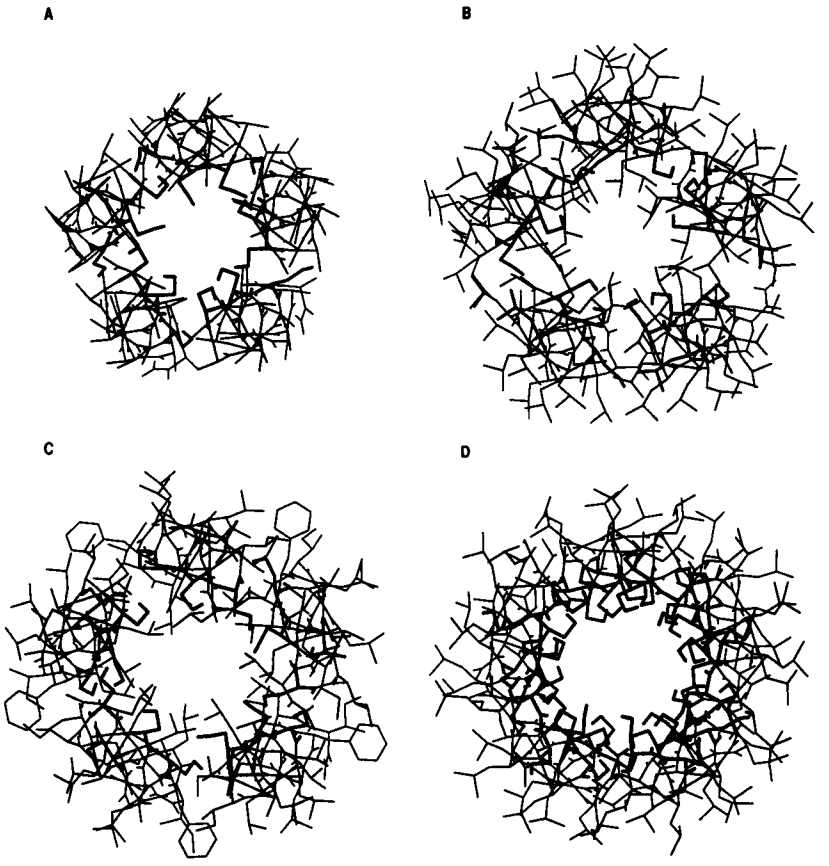

FIGURE 7 Amphipathic helix bundles. The most symmetrical helix bundle structures for amphipathic models M2aN5R6 (*A*), M2bN5R6 (*B*), M2cN5R6 (*C*), and LSN5R6 (*D*). Polar residues are highlighted using bold lines. The view is down z from the N-termini towards the C-termini.

TABLE 5 Amphipathic TM helix bundles

Model	$\langle\Omega\rangle$ (°)	$\langle D\rangle$ (Å)	$\langle\Delta E_{VDW}\rangle$ (kcal/mol)	$\langle\Delta E_{ES}\rangle$ (kcal/mol)
M2aN5R6	+4.6 (6.5)	8.1 (0.3)	−117.4 (9.4)	−12.3 (7.3)
M2bN5R6	+5.6 (4.1)	9.6 (0.3)	−166.5 (5.8)	−8.2 (4.5)
M2cN5R6	+7.5 (4.7)	9.5 (0.7)	−154.9 (7.5)	−7.1 (3.2)
LSN4R6	+15.7 (5.4)	8.6 (0.5)	−136.4 (13.6)	−22.6 (10.3)
LSN5R6	+5.1 (7.4)	9.2 (0.6)	−146.8 (11.6)	−28.6 (8.7)
LSN6R6	+1.7 (7.4)	9.2 (0.5)	−176.5 (9.1)	−38.4 (7.7)

TABLE 6 Symmetrical TM helix bundles

Model	$\langle\Omega\rangle$ (°)	$\langle P\rangle$* (Å)	$\langle R\rangle$ (Å)	R_{MIN} (Å)	Closest contact
A_{20}N4R6	+18	161	1.1	0.6	Cβ:A-17
A_{20}N5R6	+12	234	2.2	1.7	Cβ:A-17
A_{20}N6R6	+12	245	3.3	2.3	Cβ:A-21
L_{20}N5R6	+13	283	1.8	1.3	Cδ1:L-10 & Cδ1:L-17
I_{20}N5R6	−5	−2250	2.6	1.8	Cδ:I-17
M2aN5R6	+10	572	2.5	1.3	Oγ:S-8
M2bN5R6	+11	285	2.0	1.0	Cδ2:L-19
M2cN5R6	+15	323	2.2	1.0	Cδ2:L-11
LSN5R6	+17	203	2.7	2.1	Oγ:S-20

* A positive value of P corresponds to a left-handed supercoil, and a negative value to a right-handed supercoil.

Furthermore, the distribution of crossing angles is broader for all three M2 ensembles than for the A_{20} and L_{20} ensembles. This indicates looser helix packing within the M2 ensembles. Inter-helix separations for the M2 bundles do not differ significantly from those for the corresponding hydrophobic helix bundles. The ΔE_{VDW} value for the M2a ensemble is close to that for A_{20}, but those for M2b and M2c are smaller than for L_{20}, again suggesting looser helix packing.

Somewhat surprisingly, comparison of the most symmetrical helix bundles (Table 6) does *not* reveal a significant difference in crossing angles between M2 and hydrophobic TM helix bundles. This suggests that although the presence of serine residues results in greater variability in helix packing within an ensemble, the most symmetrical bundles resemble those of hydrophobic TM helices. The pore radius profile for the representative M2c bundle (Fig. 8 *D*) reveals a less regular pattern of minima than is seen for A_{20} or L_{20}. The constriction of the pore near its N-terminal mouth (at $z \sim -3$ Å) is formed in part by the hydroxyl groups of S4 side chains. Mutagenesis studies suggest that residue 4 of M2 may correspond to the narrowest region of the open channel of nAChR (Villaroel et al., 1991). The central constriction of the M2c bundle (at $z = \sim -15$ Å) is formed by the side chains of residue L11. The radius at this point falls to 1.0 Å (i.e., less than the ionic radius of K^+), effectively occluding the pore. Residue 11 of nAChR M2 is a highly conserved leucine, which has been implicated in occluding the channel when the latter is in a closed (or desensitized) conformation (Revah et al., 1991; Unwin, 1993). Thus, the model M2c pore has several features reminiscent of the nAChR channel.

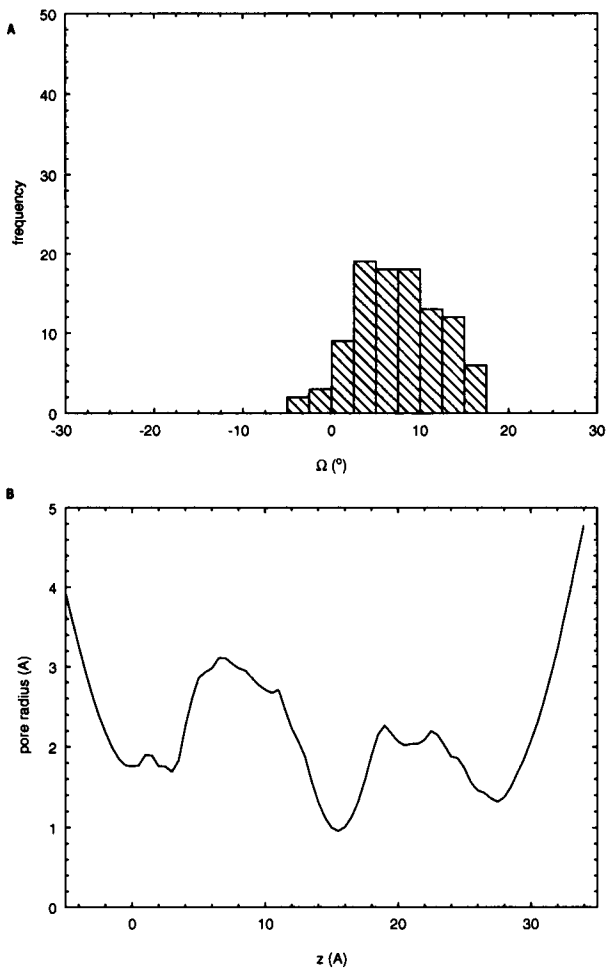

FIGURE 8 M2cN5R6 bundle. *A* shows the distribution of helix crossing angles for the ensemble of 20 structures. *B* is the pore radius profile of the most symmetrical member of the ensemble. The N-terminal mouth of the pore is at $z \sim -5$ Å and the C-terminal mouth at $z \sim 35$ Å.

It is informative to examine the patterns of serine side-chain H-bonding within M2 bundle ensembles (Table 7). Serine side chains within α-helices may H-bond to the main-chain carbonyl O of the preceding turn of the helix ($i \rightarrow i-3$ or $i-4$ H-bonds) by adopting either the g^+ or g^- conformation (Gray and Matthews, 1984). This exposes the Oγ atom of the side chain within the lining of the pore, providing a possible site for favorable interactions with permeant cations

TABLE 7 H-Bonding in amphipathic TM helix bundles

Model	Average number of H-bonds per helix		
	intra-helix	*inter*-helix (OH → OC)	*inter*-helix (OH → OH)
M2aN5R6	0.90	0.39	0.22
M2bN5R6	1.83	0.05	0.12
M2cN5R6	1.83	0.09	0.03
LSN4R6	4.99	0.68	1.18
LSN5R6	4.85	0.52	0.88
LSN6R6	4.82	0.44	0.69

(Sansom, 1992). For the M2 helices, a maximum of three such intra-helix H-bonds per helix could be formed. However, small distortions to the N-termini of the helices are likely to result in disruption of H-bonds donated by S4 hydroxyls to the carbonyl oxygens of residues 1 ($i \rightarrow i-3$) and 0 ($i \rightarrow i-4$; residue 0 is the Ace group). Thus, one might expect two intrahelical H-bonds per helix. This is indeed the case for M2b and M2c. In M2a the closer approach of the helices results in a higher frequency of *inter*-helix H-bonding, and so a lower degree of *intra*-helix H-bonding. Such inter-helix H-bonding occurs from the OH groups of the serine side chains to both main-chain carbonyl and side-chain OH groups of neighboring helices within a bundle, albeit at a relatively low frequency.

7 LS: *N* = 4, 5, and 6 bundles

Ion channels formed by CFPs, such as LS, generally exhibit multiple conductance levels, corresponding to different number of helices per bundle, N (Sansom, 1991). Thus, $N = 4$, 5, and 6 bundles of LS helices were modeled. For each model, the Cα template was constructed such that the center of the serine-containing hydrophilic face was directed towards the center of the pore. Thus, the pore is lined by the Oγ groups of the serine side chains (see Fig. 7 *D*).

The ensemble statistics for the LS bundles are given in Table 5. All three ensembles correspond to left-handed coiled coils. However, as with the M2 ensembles, the mean crossing angles are considerably less than the values exhibited by the L_{20} bundles. Also, as observed with the M2 ensembles, the Ω distributions are wider than for L_{20} (Fig. 9 *A*), indicating looser packing interactions. As N increases from 4 to 6, the ensemble mean crossing angle decreases (and, hence, the coiled coil pitch increases), such that for $N = 6$ the helices are almost parallel. The van der Waals component of the helix-helix interaction energy is ~ -30 kcal/mol/helix, compared with -40 kcal/mol/helix for L_{20}. The decrease reflects the reduced number of interdigitating leucine side chains in LS. However, this is compensated for in part by increased electrostatic helix-helix interactions (see below).

Analysis of the H-bonding patterns of the three LS ensembles is given in Table 7. Following similar arguments to those for the M2 helices, one would expect ~7 intra-helix H-bonds for each LS helix. As can be seen, about five intra-helix H-bonds are observed. However, 1 or 2 inter-helix H-bonds are also found for each helix of a bundle. Such inter-helix H-bonds are particularly frequent for serine residues 2 and 3, which cannot form intra-helix H-bonds. The relatively high frequency of inter-helix H-bonds for the LS bundles is reflected in the increased electrostatic component to the helix-helix interaction energy (ΔE_{ES}; Table 5).

The properties of the pore formed by the most symmetrical member of the LS $N = 5$ ensemble are summarized in Table 6, and the HOLE profile is given in Fig. 9 *B*. As with the M2 models, the most symmetrical LS bundle shows a crossing angle (+17°) and coiled coil pitch (203 Å) close to

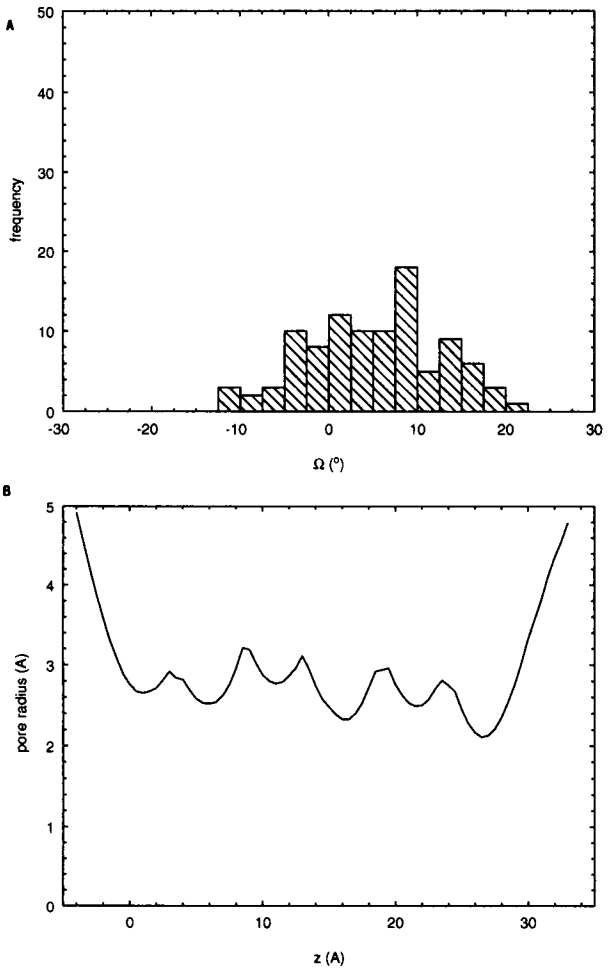

FIGURE 9 LSN5R6 bundle. *A* shows the distribution of helix crossing angles of the ensemble, and *B* shows the pore radius profile for the most symmetrical bundle.

the values for the corresponding L_{20} bundle (+13° and 283 Å, respectively). The mean radius of the pore (2.7 Å) is such that passage of monovalent cations in a partially hydrated state could occur. The minima in the pore radius profile correspond to Oγ atoms of residues S2, S6, S9, S13, S16, and S20, i.e., the same 3 or 4 residue periodicity seen in simple hydrophobic helix bundles. The narrowest region of the pore is at the C-terminus, where the closest approach is to S20:Oγ. Thus, the close interactions of serine Oγ atoms and permeant ion would be expected to confer cation selectivity on the resultant channel, as is indeed observed experimentally (Lear et al., 1988).

DISCUSSION

Evaluation of methodology

In the absence of an atomic resolution crystal structure for an ion channel formed by a parallel bundle of transbilayer helices, the success or otherwise of SA/MD in modeling such structures must be evaluated indirectly. One method of assessment is to compare helix packing in simulated bundles with helix packing in experimentally determined coiled coil structures. In particular, one may compare helix crossing angles (Ω) and coiled coil pitches (P). For A_{20} and L_{20} dimers and bundles, $\langle\Omega\rangle$ values lie in the range +12 to +20°. This compares reasonably well with Ω = +23° predicted by Chothia et al. (1981) for class 3–4 ridges-in-grooves helix packing, and is in broad agreement with a more recent survey of helix packing in protein crystal structures by Reddy and Blundell (1993). A more subtle feature of SA/MD-generated structures is the trend in coiled coil pitches. In general, P increases as N increases. Thus, for A_{20} bundles, P = 108, 161, and ~240 Å for N = 2, 4, and 5/6, respectively. Similarly, for L_{20} P = 174 and 283 Å for N = 2 and 5, respectively. A similar trend has been observed in crystal structures of coiled coils formed by peptides. The GCN4 dimer (O'Shea et al., 1991) has Ω = +23° and P = 148 Å, whereas the GCN4-derived peptide p-LI, which forms a tetrameric coiled coil (Harbury et al., 1993), has Ω = +26° and P = 205 Å. The up-up-down trimeric coiled coil formed by the peptide coil-Ser (Lovejoy et al., 1993) has Ω ~+20° and P ~270 Å. From a survey of six crystal structures, Seo and Cohen (1993) concluded that for dimeric coiled coils $\langle P\rangle$ ~150 Å (140 Å for tropomyosin), whereas for trimeric and tetrameric coiled coils $\langle P\rangle$ ~200 Å. Thus, the simulated structures of hydrophobic TM helix bundles are consistent with available experimental data on coiled coils, even though exactly parallel helices (Ω = 0°) were used in the Cα templates for the former. This helps to support the validity of the methodology. Such considerations suggest that predicted TM helix bundle structures merit detailed analysis.

One may also compare helix packing in SA/SD-generated bundles with the somewhat sparse data for ion channels. In all of the helix bundles discussed above (with the exception of I_{20}), left-handed coiled coils have been observed. This correlates with two observations on ion channel structures. First, in the 9 Å resolution structure of the closed conformation of the nAChR (Unwin, 1993), the N-terminal segments of the five M2 helices form a left-handed coiled coil, corresponding to an approximate crossing angle of +17°. Second, Åkerfeldt et al. (1993) modeled bundles of N = 3, 4, 5, and 6 LS peptide helices by a combination of interactive graphics and energy minimization. They found that left-handed coiled coils were required to obtain good inter-helical packing of side chains. Thus, LS bundle models generated by SA/MD agree quite closely with those generated by a more interactive procedure.

An aspect of the SA/MD procedure that merits discussion is the use of inter-helix distance restraints during *Stage 2*. Similar restraints were employed by Nilges and Brünger (1991) in their successful structure prediction of GCN4 helix dimers. In the current study, restraints were used to favor a packing mode corresponding to a symmetrical, open bundle surrounding a central pore. Thus, restraints were employed to focus on a region of conformational space that is believed to correspond to possible channel structures. The restraints employed were relatively soft. Furthermore, SA/MD calculations on alamethicin helix bundles (J. Breed and M. S. P. Sansom, unpublished observations) suggest that

final structures are not over-dependent on the exact value of the target distances used in the inter-helix restraints.

Simulations using only three restraints per helix, i.e., with restraints only acting between adjacent helices (H_i to H_{i+1}), resulted primarily in distorted bundles. For example, A_{20}N5R3 and L_{20}N5R3 bundles often consisted of an inner bundle of four helices, with a fifth helix running alongside. Many peptide-induced ion channels exhibit multiple conductance levels, with different conductance levels corresponding to different numbers of helices/bundle. One might speculate that distorted 4 + 1 bundles observed in the simulations may correspond to intermediates in spontaneous transitions of CFP channels between $N = 4$ and $N = 5$ conductance states.

It is evident that even when six restraints per helix are used, there is variation in the values of, e.g., Ω and D within an ensemble (see, e.g., Fig. 2 *D* for the Ω distribution of ensemble A_{20}N5R6). This reflects the extent to which noncovalent interactions between the helices, while satisfying the applied restraints, permit variations in the bundle geometry. In the absence of either extensive subunit-subunit interactions (as in the nAChR) or possible covalent restraints on helix packing (as in, e.g., template-assembled bundles of CFPs), it is perhaps not surprising that a bundle of helices does not adopt a single, exactly defined conformation. Indeed, it is possible that the relative looseness of helix-helix interactions in TM helix bundles may correlate with the observed heterogeneity of conductance levels seen for CFP channels (see Oiki et al. (1988) for a detailed analysis of such conductance heterogeneity in M2δ peptide channels).

General conclusions

A number of general conclusions may be drawn. First, consider the hydrophobic TM helices. Comparing A_{20} and L_{20}, as expected the larger side chains in the latter result in stronger van der Waals interactions between helices. This, in turn, leads to tighter packing of L_{20} helices, as evidenced by lower ensemble RMSDs and lower SDs in Ω than for A_{20}. Comparisons between dimers and $N = 5$ bundles of L_{20} suggests that packing of helices within a bundle reduces the crossing angle to some extent relative to the ideal ridges-in-grooves value of $\sim+23°$. This should be taken into account when generating α-helix bundle models of channels. Comparison of I_{20} and L_{20} indicates that β-branched residues may perturb helix packing within a bundle, resulting in smaller Ω and ΔE_{VDW} values. Such loosening of helix-helix interfaces by β-branched residues is of interest in the context of the relatively high frequency of such side chains in TM helices (Deber et al., 1986). Furthermore, a sequence motif containing β-branched side chains (LIxxGVxxGVxxT), which is present in several membrane proteins results in formation of *right*-handed coiled coils (Ω negative) of TM helices (Treutlein et al., 1992; Lemmon et al., 1994). Thus, changes in helix packing may result from quite subtle changes in TM helix sequence.

A major conclusion concerning amphipathic helix bundles is that polar residues may perturb helices from classical ridges-in-grooves packing. For example, compare ensembles A_{20}N5R6 ($\Omega = +13°$), and M2aN5R6 ($\Omega = +5°$). Polar (Ser) residues in M2a result in a small crossing angle (and, hence, increased coiled coil pitch) than in the corresponding hydrophobic TM helix bundle. This correlates with the number of *inter*-helix H-bonds made by the Ser residues, as may be shown by comparison of M2a, M2b, and M2c. The number of inter-helix H-bonds is greater in M2a because the smaller side chains (Ala rather than Leu, etc.) allows closer approach of adjacent helices. Perturbation of hydrophobic helix packing by polar side chains is also seen in the LS peptide models (Tables 5 and 7) in models of helix bundles formed by nAChR M2 helices (R. Sankararamakrishnan and M. S. P. Sansom, unpublished observations) and in alamethicin channel models (J. Breed and M. S. P. Sansom, unpublished observations). A more detailed treatment of such H-bonding interactions between adjacent helices will require modeling of water molecules within the central pore. Current studies are focusing on this problem in the context of nAChR M2 and alamethicin channels.

Relevance of these studies

What is the relevance of modeling bundles of simple hydrophobic and amphipathic helices to understanding real ion channels? Studies on simple model helices reveal general architectural principles of parallel helix bundles. Observed deviations from the simple structures described above may aid in identification of key amino acids in more complex systems. For example, our investigations of simple amphipathic helices suggest that introduction of polar residues, in addition to providing a hydrophilic lining for the central pore, may result is smaller helix crossing angles than in bundles of apolar helices. Comparable studies on bundles of nAChR M2 helices, which contain ionized side chains in addition to Ser and Thr, suggest that stronger electrostatic interactions cause even greater deviations from classical ridges-in-grooves packing (R. Sankararamakrishnan and M. S. P. Sansom, unpublished observations).

An argument against the relevance of simple model bundles is that ion channel proteins exhibit more complex bundle structures, e.g., kinked pore-lining helices. Kinked M2 helices have been observed in the nAChR when the latter is a *closed* conformation (Unwin, 1993). However, it is possible that the degree of kink of the M2 helices may be reduced when the channel changes to an *open* conformation. Indeed, MD simulations of isolated M2 helices suggest that M2 switches between linear and kinked conformations, dependent on the pattern of side-chain-backbone H-bonding (Sankararamakrishan and Sansom, 1994). More permanent kinks in-channel-lining helices may be induced by proline residues, as in alamethicin (Fox and Richards, 1982; Sansom, 1993a, b), and in the S6 helix of voltage-gated K^+ channels. SA/MD has been used to model helix bundles formed by proline-kinked alamethicin helices (Breed and Sansom, 1994) and to analyze the extent of kinking of *Shaker* S6 by the central Pro-Val-Pro motif (I. D. Kerr and M. S. P. Sansom, unpublished observations). Thus, the methodology

established in this study may be readily adapted to more complex channel structures.

Helix bundles and ion channels

Two features of helix bundle structures are of particular relevance to ion channels: (a) pore radius profiles, and (b) analysis of pore-lining side chains.

It is informative to compare the radii of pores formed by bundles of simple hydrophobic TM helices with those of other ion channels. For example, $N = 5$ bundles of A_{20} and of L_{20} have mean pore radii ~2.2 and 1.8 Å, and minimum radii of ~1.7 and 1.3 Å, respectively. Thus, either pore is wide enough to permit passage of, e.g., an unhydrated K^+ ion (radius 1.3 Å). This may be compared with the $\leftrightarrow\beta^{6.3}$ model of the gramicidin A (GA) channel (analyzed by Smart et al. (1993), which has a mean pore radius of ~1.5 Å and minimum radius of 1.2 Å, and which conducts caesium and smaller monovalent cations. Thus, $N = 5$ bundles of parallel α-helices generate wider pores than does GA, even before one takes into account, e.g., the presence of small polar side chains in the pore lining.

Two interesting features emerge from analysis of pore radii of hydrophobic TM helix bundles. The first is that even in simple models, rings of pore-lining side chains are evident, with a 3- or 4-residue periodicity. This echoes the results of mutagenesis studies of nAChR (reviewed by Bertrand et al., 1993), which provide experimental evidence for such pore-lining rings. In the N-terminal half of M2, mutagenesis studies have implicated side chains 1′, 4′, 8′, 11′, and 12′ (where the numbering refers to the position within the M2 helix) as pore-lining residues, i.e., also showing a 3- or 4-residue periodicity. Second, our simulations suggest that relatively small distortions to the termini of the helices (where packing interactions are weaker) can result in significant narrowing of the pores. This is evocative of a possible gating mechanism via small conformational rearrangements at the mouth(s) of a channel. However, there are considerable limitations to our models. For example, the mean radius of the M2c $N = 5$ bundle is ~2.2 Å (cf. 1.8 Å for L_{20}), albeit with a pronounced constriction in the vicinity of residue L11. However, electrophysiological studies suggest a pore radius of ~3.3 Å for the nAChR (Hille, 1992). Thus, the M2c bundle model requires considerable modification to provide an accurate representation of the nAChR pore.

Other information from modeling studies of relevance to ion channels concerns the role of inter-helix H-bonds in stabilizing amphipathic helix bundles. Results with M2-like sequences suggest that inter-helix H-bonding occurs at a low but significant frequency. Only when the number of polar side chains is considerably increased, e.g., in the LS peptide, is H-bond formation a significant component of bundle stabilization energies. Thus, it is unclear whether inter-helix H-bonds are likely to play a major stabilizing role in ion channels in general.

Our thanks go to the Oxford Centre for Molecular Sciences for access to computational facilities.

This work was supported by a grant from the Wellcome Trust.

REFERENCES

Adamson, J. G., N. E. Zhou, and R. S. Hodges. 1993. Structure, function and application of the coiled-coil protein folding motif. *Curr. Opin. Biotechnol.* 4:428–437.

Åkerfeldt, K. S., J. D. Lear, Z. R. Wasserman, L. A. Chung, and W. F. DeGrado. 1993. Synthetic peptides as models for ion channel proteins. *Acc. Chem. Res.* 26:191–197.

Baker, E. N., and R. E. Hubbard. 1984. Hydrogen bonding in globular proteins. *Prog. Biophys. Mol. Biol.* 44:97–179.

Bertrand, D., J. L. Galzi, A. Devillers-Thiéry, S. Bertrand, and J. P. Changeux. 1993. Stratification of the channel domain in neurotransmitter receptors. *Curr. Opin. Cell Biol.* 5:688–693.

Breed, J., and M. S. P. Sansom. 1994. Alamethicin channels modelled by simulated annealing and molecular dynamics. *Biochem. Soc. Trans.* 22:157S.

Brooks, B. R., R. E. Bruccoleri, B. D. Olafson, D. J. States, S. Swaminathan, and M. Karplus. 1983. CHARMM: a program for macromolecular energy, minimization, and dynamics calculations. *J. Comp. Chem.* 4:187–217.

Brünger, A. T. 1993. X-PLOR, Version 3.1, A system for X-ray crystallography and NMR. Yale University Press, New Haven, CT.

Changeux, J. P., J. I. Galzi, A. Devillers-Thiéry, and D. Bertrand. 1992. The functional architecture of the acetylcholine nicotinic receptor explored by affinity labelling and site-directed mutagenesis. *Q. Rev. Biophys.* 25:395–432.

Charnet, P., C. Labarca, R. J. Leonard, N. J. Vogelaar, L. Czyzyk, A. Gouin, N. Davidson, and H. A. Lester. 1990. An open-channel blocker interacts with adjacent turns of α-helices in the nicotinic acetylcholine receptor. *Neuron.* 2:87–95.

Chothia, C. 1984. Principles that determine the structure of proteins. *Ann. Rev. Biochem.* 53:537–572.

Chothia, C., M. Levitt, and D. Richardson. 1981. Helix to helix packing in proteins. *J. Mol. Biol.* 145:215–250.

Chou, K. C., G. Némethy, and H. A. Scheraga. 1984. Energetic approach to the packing of α-helices. 2. General treatment of nonequivalent and nonregular helices. *J. Am. Chem. Soc.* 106:3161–3170.

Chou, K. C., and L. Carlacci. 1991. Simulated annealing approach to the study of protein structures. *Protein. Eng.* 4:661–667.

Cohen, C., and D. A. D. Parry. 1994. α-Helical coiled coils: More facts and better predictions. *Science.* 263:488–489.

Cohen, C., and D. A. D. Parry. 1990. α-Helical coiled coils and bundles: How to design an α-helical protein. *Proteins Struct. Funct. Genet.* 7:1–15.

Deber, C. M., C. J. Brandl, R. B. Deber, L. C. Hsu, and X. K. Young. 1986. Amino acid composition of the membrane and aqueous domains of integral membrane proteins. *Arch. Biochem. Biophys.* 251:68–76.

DeGrado, W. F., Z. R. Wasserman, and J. D. Lear. 1989. Protein design, a minimalist approach. *Science.* 243:622–628.

Eisenman, G., and O. Alvarez. 1991. Structure and function of channels and channelogs as studied by computational chemistry. *J. Membr. Biol.* 119: 109–132.

Furois-Corbin, S., and A. Pullman. 1986a. Theoretical study of the packing of α-helices by energy minimization: effect of the length of the helices on the packing energy and on the optimal configuration of a pair. *Chem. Phys. Lett.* 123:305–310.

Furois-Corbin, S., and A. Pullman. 1986b. Theoretical study of the packing of α-helices of poly(L-alanine) into transmembrane bundles. Possible significance for ion transfer. *Biochim. Biophys. Acta.* 860:165–177.

Furois-Corbin, S., and A. Pullman. 1987. Theoretical study of the packing of α-helices into possible transmembrane bundles: sequences including alanines, leucines and serines. *Biochim. Biophys. Acta.* 902:31–45.

Gazit, E., D. Bach, I. D. Kerr, M. S. P. Sansom, N. Chejanovsky, and Y. Shai. 1994. The α-5 segment of *Bacillus thurigiensis* δ-endotoxin: in vitro activity, ion channel formation and molecular modelling. *Biochem. J.* In press.

Giraudat, J., M. Dennis, T. Heidmann, P. Y. Haumont, F. Lederer, and J. P. Changeux. 1987. Structure of the high-affinity binding site for noncompetitive blockers of the acetylcholine receptor: [^{3}H] chlorpromazine labels homologous residues in the β and δ chains. *Biochemistry.* 26:2410–2418.

Gray, T. M., and B. M. Matthews. 1984. Intrahelical hydrogen bonding of serine, threonine and cysteine residues within α-helices and its relevance to membrane-bound proteins. *J. Mol. Biol.* 175:75–81.

Grove, A., M. Mutter, J. E. Rivier, and M. Montal. 1993. Template-assembled synthetic proteins designed to adopt a globular, 4-helix bundle conformation form ionic channels in lipid bilayers. *J. Am. Chem. Soc.* 115:5919–5924.

Harbury, P. B., T. Zhang, P. S. Kim, and T. Alber. 1993. A switch between two-, three-, and four-stranded coiled coils in GCN4 leucine zipper mutants. *Science.* 262:1401–1407.

Hille, B. 1992. Ionic Channels of Excitable Membranes, 2nd. ed. Sinauer Associates, Sunderland, MA.

Hucho, F., W. Oberthür, and F. Lottspeich. 1986. The ion channel of the nicotinic acetylcholine receptor is formed by the homologous helices M II of the receptor subunits. *FEBS Lett.* 205:137–142.

Jähnig, F., and O. Edholm. 1992. Modelling of the structure of bacteriorhodopsin—a molecular dynamics study. *J. Mol. Biol.* 226:837–850.

Kerr, I. D., and M. S. P. Sansom. 1993. Hydrophilic surface maps of α-helical channel-forming peptides. *Eur. Biophys. J.* 22:269–277.

Kerr, I. D., R. Sankararamakrishnan, and M. S. P. Sansom. 1994. Simplified models of the pore domain of the nicotinic acetylcholine receptor. *Biochem. Soc. Trans.* 22:158S.

Kienker, P. K., W. F. DeGrado, and J. D. Lear. 1994. A helical-dipole model describes the single-channel current rectification of an uncharged peptide ion channel. *Proc. Natl. Acad. Sci. USA.* 91:4859–4863.

Kraulis, P. J. 1991. MOLSCRIPT: a program to produce both detailed and schematic plots of protein structures. *J. Appl. Cryst.* 24:946–950.

Lear, J. D., Z. R. Wasserman, and W. F. DeGrado. 1988. Synthetic amphiphilic peptide models for protein ion channels. *Science.* 240:1177–1181.

Lemmon, M. A., H. R. Treutlein, P. D. Adams, A. T. Brünger, and D. M. Engelman. 1994. A dimerization motif for transmembrane α-helices. *Struct. Biol.* 1:157–163.

Leonard, R. J., C. G. Labarca, P. Charnet, N. Davidson, and H. A. Lester. 1988. Evidence that the M2 membrane-spanning region lines the ion channel pore of the nicotinic receptor. *Science.* 242:1578–1581.

Lester, H. 1992. The permeation pathway of neurotransmitter-gated ion channels. *Annu. Rev. Biophys. Biomol. Struct.* 21:267–292.

Li, S. C., and C. M. Deber. 1992. Glycine and β-branched residues support and modulate peptide helicity in membrane environments. *FEBS Lett.* 311:217–220.

Li, S. C., and C. M. Deber. 1994. A measure of helical propensity for amino acids in membrane environments. *Nature Struct. Biol.* 1:368–373.

Lovejoy, B., S. Choe, D. Cascio, D. K. McRorie, W. F. DeGrado, and D. Eisenberg. 1993. Crystal structure of a triple-stranded α-helical bundle. *Science.* 259:1288–1293.

Lupas, A., M. van Dyke, and J. Stock. 1991. Predicting coiled coils from protein sequences. *Science.* 252:1162–1164.

McGregor, M. J., S. A. Islam, and M. J. E. Sternberg. 1987. Analysis of the relationship between side-chain conformation and secondary structure in globular proteins. *J. Mol. Biol.* 198:295–310.

Mellor, I. R., D. H. Thomas, and M. S. P. Sansom. 1988. Properties of ion channels formed by *Staphylococcus aureus* δ-toxin. *Biochim. Biophys. Acta.* 942:280–294.

Montal, M. 1990. Molecular anatomy and molecular design of channel proteins. *FASEB J.* 4:2623–2635.

Montal, M. O., T. Iawmoto, J. M. Tomich, and M. Montal. 1993. Design, synthesis and functional characterization of a pentameric channel protein that mimics the presumed pore structure of the nicotinic cholinergic receptor. *FEBS Lett.* 320:261–266.

Nilges, M., and A. T. Brünger. 1991. Automated modelling of coiled coils: application to the GCN4 dimerization region. *Protein Eng.* 4:649–659.

Nilges, M., and A. T. Brünger. 1993. Successful prediction of the coiled coil geometry of the GCN4 leucine zipper domain by simulated annealing: comparison to the X-ray structure. *Proteins Struct. Funct. Genet.* 15:133–146.

O'Shea, E. K., J. D. Klemm, P. S. Kim, and T. Alber. 1991. X-ray structure of the GCN4 leucine zipper, a two-stranded, parallel coiled coil. *Science.* 254:539–544.

Oiki, S., W. Danho, V. Madison, and M. Montal. 1988. M2δ, a candidate for the structure lining the ionic channel of the nicotinic acetylcholine receptor. *Proc. Natl. Acad. Sci. USA.* 85:8703–8707.

Oiki, S., V. Madison, and M. Montal. 1990. Bundles of amphipathic transmembrane α-helices as a structural motif for ion-conducting channel proteins: studies on sodium channels and acetylcholine receptors. *Proteins Struct. Funct. Genet.* 8:226–236.

Oliver, A. E., and D. W. Deamer. 1994. α-Helical hydrophobic polypeptides form proton-selective channels in lipid bilayers. *Biophys. J.* 66:1364–1379.

Phillips, G. N. 1992. What is the pitch of the α-helical coiled coil? *Proteins Struct. Funct. Genet.* 14:425–429.

Raghunathan, G., P. Seetharamulu, B. R. Brooks, and H. R. Guy. 1990. Models of δ-hemolysin membrane channels and crystal structures. *Proteins Struct. Funct. Genet.* 8:213–225.

Reddy, B. V. B., and T. L. Blundell. 1993. Packing of secondary structure elements in proteins: analysis and prediction of inter-helix distances. *J. Mol. Biol.* 233:464–479.

Revah, F., D. Bertrand, J. L. Galzi, A. Devillers-Thiery, C. Mulle, N. Hussy, S. Bertrand, M. Ballivet, and J. P. Changeux. 1991. Mutations in the channel domain alter-desensitization of a neuronal nicotinic receptor. *Nature.* 353:846–849.

Rozzelle, J. E., A. Tropsha, and B. W. Erickson. 1994. Rational design of a three-heptad coiled-coil protein and comparison by molecular dynamics simulation with the GCN4 coiled coil: presence of interior three-center hydrogen bonds. *Protein Sci.* 3:345–355.

Sankararamakrishnan, R., and M. S. P. Sansom. 1994. Kinked structures of isolated nicotinic receptor M2 helices: a molecular dynamics study. *Biopolymers.* In press.

Sansom, M. S. P. 1991. The biophysics of peptide models of ion channels. *Prog. Biophys. Mol. Biol.* 55:139–236.

Sansom, M. S. P. 1992. An investigation of the role of serine and threonine sidechains in ion channel proteins. *Eur. Biophys. J.* 21:281–298.

Sansom, M. S. P. 1993a. Alamethicin and related peptaibols—model ion channels. *Eur. Biophys. J.* 22:105–124.

Sansom, M. S. P. 1993b. Structure and function of channel-forming peptaibols. *Q. Rev. Biophys.* 26:365–421.

Sansom, M. S. P. 1993c. Acetylcholine receptor: peering down a pore. *Curr. Biol.* 3:239–241.

Sansom, M. S. P., and I. D. Kerr. 1993. Influenza Virus M_2 Protein: a molecular modelling study of the ion channel. *Protein Eng.* 6:65–74.

Schulz, G. E., and R. H. Schirmer. 1979. *Principles of Protein Structure.* Springer-Verlag, Heidelberg, Germany.

Seo, J., and C. Cohen. 1993. Pitch diversity in α-helical coiled coils. *Proteins Struct. Funct. Genet.* 15:223–234.

Sippl, M. J. 1990. Calculations of conformational ensembles from potentials of mean force: an approach to the knowledge-based prediction of local structures in globular proteins. *J. Mol. Biol.* 213:859–883.

Smart, O. S., J. M. Goodfellow, and B. A. Wallace. 1993. The pore dimensions of gramicidin A. *Biophys. J.* 65:2455–2460.

Stroud, R. M., M. P. McCarthy, and M. Shuster. 1990. Nicotinic acetylcholine receptor superfamily of ligand gated ion channels. *Biochemistry.* 50:1107–11023.

Treutlein, H. R., M. A. Lemmon, D. M. Engelmann, and A. T. Brünger. 1992. The glycophorin A transmembrane domain dimer: sequence-specific propensity for a right-handed supercoil of helices. *Biochemistry.* 31:12726–12733.

Unwin, N. 1993. Nicotinic acetylcholine receptor at 9 Å resolution. *J. Mol. Biol.* 230:1101–1124.

Unwin, N. 1989. The structure of ion channels in membranes of excitable cells. *Neuron.* 3:665–676.

Villarroel, A., S. Herlitze, M. Koenen, and B. Sakmann. 1991. Location of a threonine residue in the α-subunit M2 transmembrane segment that determines the ion flow through the acetylcholine receptor channel. *Proc. R. Soc. Lond. B.* 243:69–74.

Weiner, S. J., P. A. Kollman, D. A. Case, U. C. Singh, C. Ghio, G. Alagona, S. Profeta, and P. Weiner. 1984. A new force field for molecular mechanical simulation of nucleic acids and proteins. *J. Am. Chem. Soc.* 106:765–784.

Zhang, L., and J. Hermans. 1993. Molecular dynamics study of the structure and stability of a model coiled coil. *Proteins Struct. Funct. Genet.* 16:384–392.